Title
Comparative Visualization for Wave-based and Geometric Acoustics

Authors
Deines, Eduard
Bertram, Martin
Mohring, Jan
et al.

Publication Date
2006

Peer reviewed

Comparative Visualization for Wave-based and Geometric Acoustics

Eduard Deines, Martin Bertram, Jan Mohring, Jevgenij Jegorovs, Frank Michel, Hans Hagen, and Gregory M. Nielson

Abstract—We present a comparative visualization of the acoustic simulation results obtained by two different approaches that were combined into a single simulation algorithm. The first method solves the wave equation on a volume grid based on finite elements. The second method, phonon tracing, is a geometric approach that we have previously developed for interactive simulation, visualization and modeling of room acoustics. Geometric approaches of this kind are more efficient than FEM in the high and medium frequency range. For low frequencies they fail to represent diffraction, which on the other hand can be simulated properly by means of FEM. When combining both methods we need to calibrate them properly and estimate in which frequency range they provide comparable results. For this purpose we use an acoustic metric called gain and display the resulting error. Furthermore we visualize interference patterns, since these depend not only on diffraction, but also exhibit phase-dependent amplification and neutralization effects.

Index Terms—acoustic simulation, comparative visualization, ray tracing, finite element method, phonon map

1 Introduction

Despite the obvious dissimilarity between our aural and visual senses, many techniques required for the visualization of photo-realistic images and for the auralization of acoustic environments are quite similar. Both applications can be served by geometric methods such as particle- and ray tracing if we neglect a number of less important effects.

Recall the differences between light and acoustics: The visible spectrum is located between 400 and 700 nanometers of wavelength, whereas the lengths of sound waves in the perceivable range $\Omega = [20Hz, 20kHz]$ are located roughly between 17mm and 17m. For this reason, diffraction plays a greater role for sound, i.e. in particular low frequencies do not spread linearly but also distribute around corners and are not affected by smaller obstacles. Diffraction turns the localization of sound sources into a challenging problem. In addition, sound waves are mostly reflected in a specular way even at rough surfaces, since the greater wavelengths are not sensible to micro facets. On a coarser scale, for example when modeling thousands of chairs in a concert hall, bi-directional reflection distribution functions appear to be useful for acoustics, as well.

Human visual receptors can distinguish only three different basis colors (red / green / blue). But, what is the acoustic "color" of a material? It can be described by a frequency-dependent absorption function which is smooth in most cases and thus can be represented by few coefficients. Thus, it appears to be harder to "hear" the acoustic colors of objects rather than seeing their real colors, despite of the fact that we can precisely distinguish between different frequencies.

By means of the simulation of room acoustics we want to predict the acoustic properties of a virtual model. For auralization, a pulse response filter needs to be assembled for each pair of source and listener positions. The convolution of this filter with an anechoic source signal provides the signal received at the listener positions. Hence, the pulse response filter must contain all reverberations (echos) of a unit pulse, including their frequency decompositions due to different absorption coefficients.

In a previous work, we developed a simulation method named *phonon tracing*, [4] since it is based on particles. This method is also useful for the visualization of wave fronts and for analyzing of the impact of virtual geometries equipped with acoustic properties [7]. Like other approaches to geometric acoustics [16, 1, 8], our method computes the energy decomposition for each phonon sent out from a sound source and uses this in a second pass (phonon collection) to construct the response filters for different listeners. The attenuation of energy, which is inversely proportional to the squared distance, matches the density of particles when spreading out from a spherical source.

In order to support and understand the effect of diffraction, we present a novel algorithm for FEM-based solution of the wave equation, applicable to real time auralization. To reduce the computational complexity, we derive a state-space system representing the relevant eigenmodes. The degree of excitation of these modes is updated by each new input sample. However, as the grid size has to be smaller than the wave length FEM is restricted to the lower frequency spectrum.

When combining both methods, we need to know in which range of frequencies (relative to the scale of a virtual model) the results of both methods match. Furthermore we need to calibrate these methods and derive an error estimate based on a comparison. The present paper is concerned with this task. In particular, we make the following contributions:

- We improve the phonon tracing method by taking into account pressure rather than energy. This allows a better comparison with FEM, which is also based on pressure calculation, and accounts for interference phenomena. The linear pressure attenuation (in contrast to quadratic attenuation for energy) is modeled by Gaussian basis functions that are dilated proportional with the traversed distance. This way we approximately conserve partition of unity for our basis functions.

- We present a novel FEM-based solver for the simulation of diffraction at low frequency bands. The anechoic source signal is then separated into mid to high frequencies processed by the improved phonon tracing and low frequencies processed by our derived state-space model.

- We present a comparative visualization of interference patterns obtained by both methods (see 7). Interference occurs when multiple pressure fields are added, causing amplification in some and

- *Eduard Deines (E-mail: e_deines@informatik.uni-kl.de) and Frank Michel (E-mail: michel@informatik.uni-kl.de) are with IRTG Kaiserslautern, Germany.*
- *Martin Bertram is with DFKI Kaiserslautern, Germany, E-mail: bertram@informatik.uni-kl.de.*
- *Jan Mohring (E-mail: jan.mohring@itwm.fraunhofer.de) and Jevgenij Jegorovs (E-mail: jegorovs@itwm.fraunhofer.de) are with ITWM Kaiserslautern, Germany.*
- *Hans Hagen is with University of Kaiserslautern, Germany, E-mail: hagen@informatik.uni-kl.de.*
- *Gregory M. Nielson is with Arizona State University, USA, E-mail: nielson@asu.edu.*

Manuscript received 31 March 2006; accepted 1 August 2006; posted online 6 November 2006.

For information on obtaining reprints of this article, please send e-mail to: tvcg@computer.org.

neutralization in other regions. This cannot be done with energy distributions, since these are non-negative (proportional to squared pressure). For comparison, we use standard metrics like *gain*, equivalent to relative energy on a logarithmic scale.

The remainder of our work is structured as follows: In section 2 we review previous work. Section 3 contains the improved phonon map and our FEM-based solver. Comparative visualization results and their evaluation are provided in section 4.

2 Previous Work

In the theory of acoustics there are two main approaches simulating the propagation of sound. The first approach is based on wave equations that are numerically solved, for example using finite element methods (FEM). The simulation results are very accurate, but the complexity increases drastically with the highest frequency considered, since a volume grid with $O(n^3)$ cells needs to be constructed where n is proportional to the highest frequency. The time complexity for solving this is typically $O(n^3\ log\ n^3)$. Hence, the wave model is suitable for low frequencies only.
The second approach, known as geometric acoustics, describes the sound propagation by sound particles moving along a directed ray. There exists a variety of such methods for simulating room acoustics. They are mostly based on optical fundamentals, and make use of approaches developed there. Two classical methods for acoustic simulation are the image-source method [1, 5] and the raytracing method [16, 17]. Due to the shortcomings of the two classical approaches, continuative methods have been developed in recent years. Mostly, they employ parts of the classical schemes or a combination of them. One approach that makes use of advantages of image-source method and raytracing is introduced in [21]. Here the visibility check of the image-source algorithm are performed via raytracing. Beam-tracing methods [8, 9, 18] overcome the aliasing problem of classical raytracing by recursively tracing pyramidal beams, implying the need for highly complex geometric operations, still ignoring diffraction effects at low frequencies. Other approaches utilizing the photon mapping [11] also exist [13].

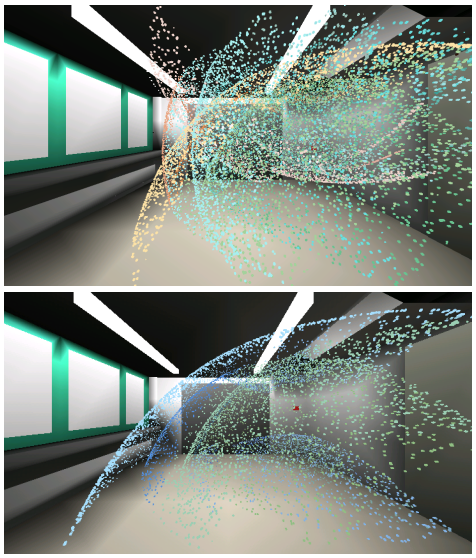

Fig. 1. Visualization of sound wave propagation. (a) different wave fronts. (b) reflections on the bottom.

Our phonon tracing approach [4] precomputes particle traces and records the phonons' direction and energy at reflecting surfaces for the collection phase. The particles contribute to the room impulse response at given listener positions. Additionally, we visualize the sound wave propagation by use of color coded spheres representing particular phonons. The color of these spheres corresponds to the energy decomposition of the phonons. An option to visualize only wave fronts reflecting from one selected material was provided (see figure 1).
In another work [7] we present different visualizations of the phonon map. The first three techniques visualize the wave fronts on the scene surfaces independent of listener position. First of all we rendered phonons as color coded spheres at their positions on reflecting surfaces. Furthermore, we visualize the outgoing direction of different particles by use of cones. In the second method we visualized the sound wave fronts reflecting from different materials by use of triangulated surfaces, which are deformed according to the traversed distance of the phonons contributing to this wave front. In the third visualization method we represented the energy distribution on a given scene surface by means of scattered data interpolation. All three methods provide the option to render the energy considering the overall frequency spectrum or the energy of only one selected frequency band. Energy is color coded using the RGB color space in the first case and the HSV color space in the second case. Additionally to the methods described above, we visualized the energy received at a given listener position. Therefore we render a color coded sphere at the listener position deformed according to the direction and amount of the arrived energy. These visualization approaches allow the visual representation of the phonon map on the scene surfaces as well as the representation of the energy received by a listener. Figure 2 shows the visualization results of the described techniques.
The methods described above are all based on the phonon map. Since we combine this method with FEM, we want to study the behavior of both methods in the overlapping frequency domain to estimate how they relate to each other.

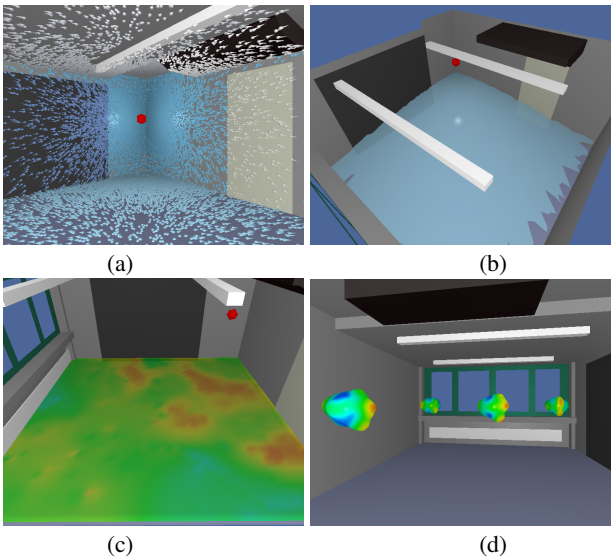

Fig. 2. Visualization of phonon map. (a) phonons on surfaces. (b) wave front visualization. (c) scattered data interpolation. (d) listener-based visualization.

3 Acoustic Simulation

3.1 Improved Phonon Tracing

In this section we present an improved phonon tracing approach, where we use sound pressure for calculations, instead of energy. The idea is analogous to [4] to trace sound particles outgoing from the sound source through the given scene building the phonon map. Afterwards the phonons are collected in order to calculate a room impulse response at a given listener position.
Our simulation algorithm requires the following input information:

- position of sound source s
- one ore more listener positions l_i

- a triangulated scene with tagged materials m_j
- an absorption function $\alpha_j : \Omega \mapsto (0,1]$ for each material
- a number of phonons n_{ph} traced from the source
- a lower pressure threshhold ε and a maximum number of reflections n_{refl} for terminating the phonon paths

The output of our approach is a FIR filter f_i for each listener's position l_i corresponding to the impulse response with respect to the sound source and the phonon-map containing for each phonon ph the pressure spectrum p_{ph}, the phonon's position pt_{ph} at the reflection point, the image source q_{ph} from which we can calculate phonons outgoing direction v_{ph} and the traversed distance d_{ph}, number of reflections r_{ph}, and the material m_{ph} at the current reflection.
Our simulation algorithm consists of two steps: the *phonon tracing* step constructs the phonon map, and the *phonon collection and filtering* step collects the phonon's contribution to a FIR filter for every listener position.

Phonon tracing. Every phonon ph emitted from the sound source carries the following information:

- a pressure spectrum $p_{ph} : \Omega \mapsto \mathbb{R}^+$
- the virtual source q_{ph}
- the phonon's current position pt_{ph}

Our absorption and pressure functions α_j are represented by $n_e = 10$ coefficients associated with the frequencies $40, 80, 160, ..., 20480$ Hz. The basis function for the pressure spectrum are wavelets adding up to a unit impulse. Every phonon is composed of different frequencies, which is more efficient than tracing a single phonon for each individual frequency band.
Phonons are emitted from the source s according to the emission probability distribution E and have at their starting point a unit pressure spectrum $p_{ph,i} = 1$ $(i = 1, ..., n_e)$. At the intersection of the phonon ray with the scene, the virtual source q_{ph} is calculated as follows:

$$q_{ph} \quad \leftarrow \quad q_{ph} + 2 \cdot \langle (pt_{ph} - q_{ph}), n \rangle \cdot n \tag{1}$$

where n is the surface normal at the intersection point pt_{ph}. The pressure is reduced according to the absorption coefficients of the local material m_j. The phonon is fixed at the intersection point, contributing to a global phonon map.
If the maximum pressure of the phonon's spectrum still exceeds the pressure threshold, i.e. $max\{p_{ph,i}\}_{i=1}^{n_e} > \varepsilon$ and a maximum number of reflections is not reached, the next phonon re-uses the path and the pressure of the preceding one, saving computation time. It is started at the current position with respect to the outgoing direction d_{ph} and contributes to the phonon map at the next surface intersection. If the threshold is not exceeded and a minimum number of reflections have been computed, then a new phonon is started from the source. After we have traced n_{ph} phonons from the source or a prescribed number of phonons have contributed on the global phonon map, the tracing is terminated.

Phonon collection and filtering. The remaining task of the phonon tracing method is collecting the phonon's contribution to a impulse response filter f for every listener's position l.
In the case of a point source and uniform absorption for all frequencies, the contribution of a phonon visible from the listener is simply a scaled, translated unit pulse (Dirac). The Dirac is shifted by the time elapsed between emission and reception of a phonon. The scaling decreases with the accumulated length and wall absorption along the phonon path and depends on the angle between the phonon direction and the direction from the virtual source to the listening point:

$$\begin{aligned} p(t,x) \quad = \quad & \frac{\rho_{tot}\, p_0}{d_{ph}}\, w\Big(\angle\left(v_{ph}, x - q_{ph}\right)\Big) \\ & \times \delta_{f_s}\left(t - \frac{d_{ph}}{c}\right) \end{aligned} \tag{2}$$

where p_0 is a reference pressure at 1m from the source, ρ_{tot} is the product of the reflection coefficients along the phonon path and w is a Gaussian weighting function designed in such a way that for equally distributed phonon directions on the unit sphere the associated Gaussian approximate a partition of unity:

$$w(\phi) = \frac{2}{n_{ph}\sigma^2} \mathrm{e}^{-\frac{\phi^2}{2\sigma^2}}. \tag{3}$$

Choosing σ there is a trade off between smoothness of the partition of unity and resolution of geometric details of the scene. The discrete Dirac impulse for sampling rate f_{s} is defined as

$$\delta_{f_{\text{s}}}(t) = \begin{cases} 1 & t \in \left[0, f_{\text{s}}^{-1}\right] \\ 0 & \text{else} \end{cases}. \tag{4}$$

Since we trace pressure rather than energy in order to simulate interference phenomena, the attenuation with respect to distance $d = \left|x - q_{ph}\right|$ is proportional to d^{-1} rather than d^{-2}. Absorption coefficients α to be found in the literature refer to energy. The pressure related reflection coefficient reads:

$$\rho = \sqrt{1 - \alpha}. \tag{5}$$

In classical acoustic raytracing [16, 17], a sphere is used to collect rays at listener position. Using Gaussian beams, however, provides much smoother filters, since more phonon rays contribute to the filter.
In the more general case of frequency-dependent absorption, the unit impulse is subdivided into wavelets representing the individual frequency bands. The filter becomes then a sum of these wavelets scaled and shifted as described above. The filter design, especially the corresponding band pass filters (wavelets), is described in full detail in [4].

3.2 Finite element method (FEM)

Phonon tracing or any other method based on geometric acoustics (ray tracing, mirror image) fail in the low frequency range for two reasons:

1. Wavelengths are of the order of typical dimensions of the room. Hence, diffraction and interference can no longer be neglected.
2. Damping is typically low at low frequencies and reverberation times become too long to be represented by a convolution kernel of reasonable length.

Therefore, we have to fall back on wave acoustics to simulate the low frequency part of the sound field. The crucial question is, if there is an intermediate frequency range where both, geometric and wave based methods provide similar results, or if there remains a gap to be filled by a third method. This question will be investigated in the next section. First, we present an efficient way to use wave based methods in a transient acoustic simulation and explain, why these methods can only be applied at low frequencies.
For closed rooms the wave equation is preferably solved by the finite element method (FEM), which approximates the wave equation by a large system of ordinary differential equations (ODEs) the unknowns of which are the pressures at grid points covering the room. In general, there are by far too many unknowns to solve these systems of ODEs in real time. Hence, we need to reduce the system to a concise state-space model with similar input-output behavior in the frequency range of interest.
There are many different approaches to model reduction [2]. The common observation is that system dynamics can often be represented quite well by a superposition of a few (generalized) eigenmodes. The coefficients of these modes are the unknowns of the new reduced system. Finally, assuming samplewise constant input (e.g. acceleration of the loudspeaker membrane), the continuous state-space model is transformed into a discrete one, which can be solved in real time.
In the following we list the steps to get from the wave equation (6) to a reduced discrete state-space model (11) describing the transient

response of a room to an excursions of a loudspeaker membrane. The wave equation and associated boundary conditions read:

$$\begin{aligned} \frac{\partial^2 p}{\partial t^2} - {c_0}^2 \Delta p &= 0 \quad \text{on} \quad G \\ c_0 \frac{\partial p}{\partial n} &= -\frac{1-R}{1+R}\frac{\partial p}{\partial t} \quad \text{on} \quad \Gamma_w \\ \frac{\partial p}{\partial n} &= -\rho_0 \frac{\partial^2 x_m}{\partial t^2} \quad \text{on} \quad \Gamma_m \,. \end{aligned} \tag{6}$$

$p = p(t,x)$ denotes pressure, $c_0 = 343m/s$ the velocity of sound, and ρ_0 =1.2 kg/m the density of air at room temperature, G the interior of the room, and Γ_w and Γ_m the surfaces of walls and membrane, respectively. x_m is the excursion of the membrane and R is a reflection coefficient. It may depend on the particular wall, but is constant for all frequencies. This is a minor problem, as we use the model only for a small frequency band.
Approximating the pressure distribution by a superposition of, for instance, piecewise quadratic ansatzfunctions $p(t,x) = \sum_{i=0}^{N} p_i(t)\,\varphi_i(x)$ and integrating (6) with respect to the φ_i gives a FE model of the form:

$$\begin{aligned} M\ddot{p} + D\dot{p} + Kp &= Fu \\ y &= Pp \,. \end{aligned} \tag{7}$$

The real $N \times N$ matrices M, D, K are called mass, damping, and stiffness matrix. $p = p(t)$ is a vector composed of the coefficients p_i. $u = u(t)$ is the input, e.g. the acceleration of the membrane. F transforms this input into a force. P is a projection matrix extracting certain interesting pressures y_i.
Setting

$$\hat{x} = \begin{bmatrix} p \\ \dot{p} \end{bmatrix}, \quad \hat{E} = \begin{bmatrix} I & 0 \\ 0 & M \end{bmatrix}, \quad \hat{A} = \begin{bmatrix} 0 & I \\ -K & -D \end{bmatrix}, \quad \hat{B} = \begin{bmatrix} 0 \\ F \end{bmatrix}, \quad \textit{and} \quad \hat{C} = \begin{bmatrix} P & 0 \end{bmatrix} \tag{8}$$

the FE model may be rewritten as a generalized state-space model:

$$\begin{aligned} \hat{E}\dot{\hat{x}} &= \hat{A}\hat{x} + \hat{B}u \\ y &= \hat{C}\hat{x} \,. \end{aligned} \tag{9}$$

Assuming that $\hat{x}$ is essentially composed of the columns of a matrix $U \in \mathbb{R}^{N \times n}$, $n \ll N$, and projecting the equations on the columns of $V \in \mathbb{R}^{N \times n}$ we end up with a reduced state-space system where

$$\hat{x} = U\tilde{x}, \quad \tilde{E} = V^t \hat{E} U \,, \quad \tilde{A} = V^t \hat{A} U \,, \quad B = V^t \hat{B}, \quad \tilde{C} = \hat{C} U \,. \tag{10}$$

The columns of U and V may be found by expanding the associated transfer function $H(s) = \hat{C}(s\hat{E} - \hat{A})^{-1}\hat{B}$ about some shifts $s_j = \mathrm{i}\omega_j$. Here, we used the *rational dual Arnoldi* algorithm described in [20]. Finally, dividing the first equation of the reduced version of (9) by $\tilde{E}$ and performing a balanced truncation [22] we end up with a state-space system of typically a few hundred unknowns rather than several 10,000 degrees of freedom. Integrating the reduced version of (9) over the length Δt of one sample for constant input u_n, i.e.

$$x_n = \mathrm{e}^{\tilde{A}\Delta t} x_{n-1} + \int_0^{\Delta t} \mathrm{e}^{\tilde{A}(\Delta t - \tau)}\,\mathrm{d}\tau\, \tilde{B} u_{n-1},$$

leads to a discrete state-space system

$$\begin{aligned} x_n &= Ax_{n-1} + Bu_{n-1} \\ y_n &= Cx_n \,. \end{aligned} \tag{11}$$

Switching to a suitable basis $x_n = T\xi_n$ it is always possible to turn the system into *companion canonical form* [15], where the first $n-1$ rows of A coincide with the last $n-1$ rows of the identity matrix of order n, the last row contains the negative coefficients of the characteristic polynomial of A, and B is the n-th unit vector. Hence, updating the state vector x_n and evaluating the pressure at a certain position requires $2n$ multiplications and $2n-1$ additions.
Finally, we explain why FEM cannot be used for higher frequencies. FEM approximates the oscillating pressure field by smooth, e.g. piecewise quadratic ansatzfunctions. To resolve a wave we need at least three or four elements per wave. This leads to a FE model of about

$$N = \left(\frac{nLf}{c_0}\right)^3 \tag{12}$$

degrees of freedom, where n is the number of elements per wave, L a typical diameter of the room, f the frequency and c_0 the velocity of sound. Note that the required number of unknowns increases as the third power of the frequency!

4 Comparison Approach

4.1 Test Scenario

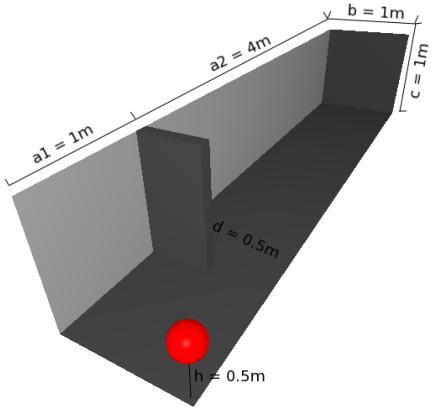

Fig. 3. Geometry of the room.

In order to compare both simulation approaches described in the previous section we consider the following test case, designed to produce interference patterns. We run the FEM and phonon tracing in a room of 5 meters length, 1 meter width, and 1 meter height with a gap of 0.5 meters (see figure 3). We place the sound source in the corner of the room. The two long walls reflect the sound wave totally, whereas the remaining room surfaces are totally absorptive. Choosing the absorption characteristics of the room in this way we model an array of sound sources as outlined in figure 4. Now we can observe interference effects as well as diffraction effects behind the gap.

Fig. 4. Simulation Scenario.

In phonon tracing we simulate the pressure inside the room on a regular grid (561 points in total). We trace 100000 phonons from the sound source in order to calculate the room impulse responses f_i at the grid points. Figure 5 shows the wave propagation from the sound source. Afterwards, for determining the pressure at a grid point g_i for a given frequency ω we convolve a sine signal of frequency ω with f_i and obtain at the position $le_{f_i} + 1$ of the resulting signal the pressure at g_i. le_{f_i} is the length of the room impulse response at i-th grid point.

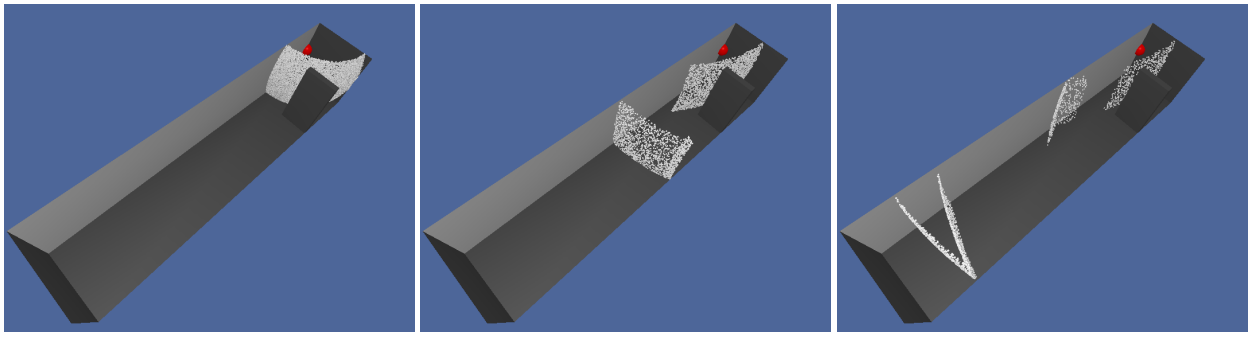

(a) (b) (c)

Fig. 5. Visualization of particle (phonons) propagation from the sound source in three consecutive time steps.

Comparing the results of phonon tracing and FEM, we consider stationary sound fields originating from a source emitting only one particular frequency. The corresponding FEM solution is computed in terms of the reduced continuous time system:

$$y(s) = \tilde{C}\left(s\tilde{E} - \tilde{A}\right)^{-1}\tilde{B} \tag{13}$$

where $s = 2\pi \mathrm{i} f$. The mean squared pressure at the i-th grid position reads:

$$p_i^2 = \frac{1}{T}\int_0^T p_i(t)^2 \mathrm{dt} = \frac{1}{2}\left|\mathrm{y_i}\right|^2 \tag{14}$$

For visualization the results are interpolated to the same grid as in phonon tracing. We have compared the simulation results for different wave numbers $k = \frac{2\pi}{\lambda} = \{3,6,9,12,15\}$ where λ is the wave length. Hence, we consider wave lengths of the order of the gap width. Note that choosing the shifts in the Arnoldi algorithm to match the above wave numbers, i.e. $s_j = ik_j c_0$, then the reduced model is exact at these wave numbers and results coinside with those of the full FEM simulation.

4.2 Interference Pattern Visualization

In the first step we have compared the pressure distributions to validate whether similar interference patterns appear. For visualization we use a quad mesh, which we color coded in the following way. We map positive pressure values to red color and negative pressure values to blue color and reduce the saturation of the color, depending on the absolute pressure value at the considering position. Additionally, all pressure values with an absolute value less than the hearing threshold level ($2 \cdot 10^{-5}$ Pa) are mapped to gray color. The resolution of the displayed mesh is higher than that of the simulation mesh, the pressure values of the additional points are then bilinearly interpolated. Figures 7 and 6 show examples of our interference pattern visualization for wave number $k = 12$ and $k = 6$, respectively. The results show that both methods faithfully reproduce matching interference patterns, where the results obtained by FEM appear to be somewhat smoother. The patterns at $k = 12$ are closer to each other than that at $k = 6$.

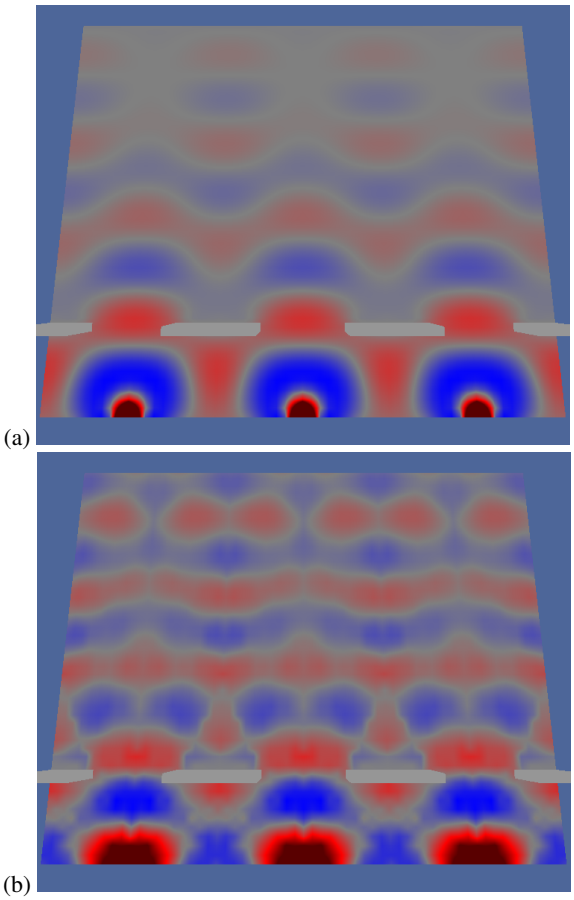

(a)

(b)

Fig. 6. Interference pattern. FEM simulation (a) and phonon tracing (b) for the wave number k=6.

Wave propagation is illustrated more intuitively, when pressures are mapped along the normal to the listening plane as shown in figure 8.

4.3 Gain Visualization

For a more detailed comparison we turn to an acoustic metric, called gain, which is essentially the logarithm of the mean squared pressure [19]:

$$G = 10log_{10}\left(\frac{\sum_{i=0}^{m} p_i^2}{\sum_{i=0}^{m} p_{10_i}^2}\right) \quad dB \tag{15}$$

Since sources have been modelled differently (point source in phonon tracing and small membrane in FEM), the sound fields are normalized by a linear fit excluding the direct neighborhood of the sources. For visualization of the gain and the error we use a quad mesh color coded from red (maximum value) to blue (minimum value). Therefore we interpolate the hue value of the HSV color space according to the gain value and error, respectively. Values for additional mesh points for rendering are bilinearly interpolated as mentioned before. To ensure better comparison feasibility, for the gain we use the same color range for different simulation types at same frequencies. Moreover, the same color range is used for all error plots. As the gain is a logarithmic measure the relative error of the pressures is proportional to the difference of the gain values and can be calculated as:

$$\varepsilon = \delta\frac{ln(10)}{20} \quad with \quad \delta = \|G_{ph_j} - G_{fem_j}\| \tag{16}$$

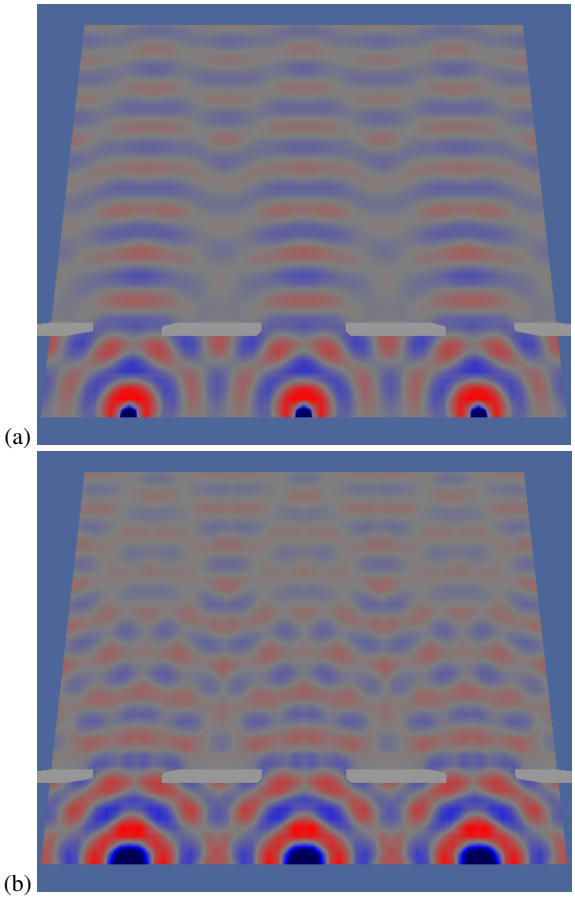

Fig. 7. Interference pattern. FEM simulation (a) and phonon tracing (b) for the wave number k=12.

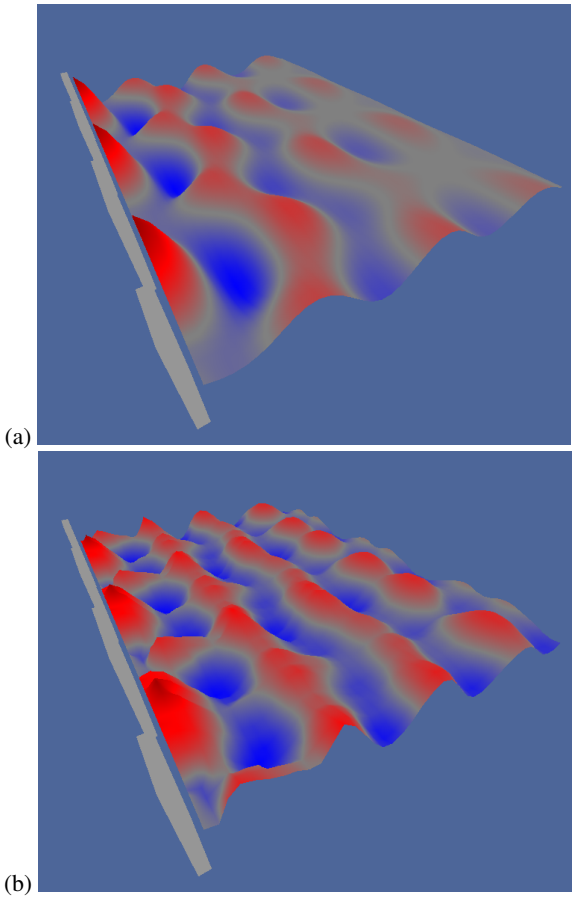

Fig. 8. Visualization of wave propagation. FEM simulation (a) phonon tracing (b) for the wave number k=6.

where G_{ph_j} and G_{fem_j} is the gain at grid point j calculated with results from phonon tracing and FEM method, respectively. Our results are summarized in table 1. We can observe a decrease of the error until $k = 12$, since the diffraction effects neglected by the phonon tracing approach become smaller. Due to the shortcomings of the FEM method at higher frequencies the error amount increases. Considering the results we can say that both simulation methods are matched best at wave number $k = 12$. In figures 9 (c), 10 (c), and 11(c) we can notice, that the blue regions on the error plots are predominant indicating overall error decrease. The gain plots of FEM and Phonon Tracing results at $k = 12$ (figure 11 (a+b)) are closer as those at $k = 3,6$ (figures 9 (a+b), 10 (a+b)). The FEM approach is the mathematically correct method in the frequency spectrum that can be represented by the grid (due to the Nyquist limit). In order to keep the calculation cost of the FEM appropriate, the wave length reaches the order of the grid size and FEM becomes inaccurate. The Phonon Tracing is the more efficient method and provide at $k = 12$ similar results as the FEM, thus we can use it for the simulation of the acoustics at the frequencies above $k = 12$, which corresponds to a wave length of half the gap width.

k	3	6	9	12	15
δ	8.216	5.164	3.989	3.784	4.903
ε	0.946	0.595	0.459	0.436	0.565

Table 1. Absolute and relative error in dB between FEM and phonon tracing.

5 Conclusions

We introduced two acoustic simulation methods, a FEM-based approach for low frequency bands and an improved phonon tracing method applicable to medium and high frequencies. The FEM-based solution is transformed into a state-space system that produces a low-frequency response signal in real time when stimulated by the anechoic source signal. Our improved phonon tracer, which is based on pressure rather than energy, accounts for interference phenomena and calculates a room impulse response for given listener positions. The fast convolution of these impulse responses with the anechoic signal issues the mid- and high-frequency components of the response signal.

In order to combine these two methods we needed to find out whether both methods produce comparable results in a certain frequency range that also needed to be estimated. With the aid of a comparative visualization for both methods we were able to find the answer to this question. Therefore we constructed a simple periodic scenario with one sound source and perfectly reflecting side walls. In the direction orthogonal to these walls we placed a short, fully absorbing wall with a gap, such that interference patterns could emerge behind this gap. We first visualize the pressure values resulting from both simulations in order to represent interference patterns. Additionally, for a more accurate comparison of the methods we turn to an acoustic metric "gain" and visualize the gain as well as the error between the results. For comparison we simulate the acoustics at different wavelength $k = \{3,6,9,12,15\}$.

The resulting images suggested that both methods were able to faithfully reproduce correct interference patterns. With our visualization we were able to figure out at witch frequency range the two methods match. The lowest discrepancy was obtained at $k = 12$, which corresponds to a wave length of half the gap size (0.5 m). For higher frequencies, the grid required by FEM soon becomes prohibitively large and for lower frequencies, the lack of diffraction reduces the fidelity of phonon tracing.

ACKNOWLEDGMENTS

This work was supported by the Stiftung Rheinland-Pfalz für Innovation under contract no. 15202-386261/644 and by the Kaiserslautern Excellence Cluster Dependable Adaptive Systems and Mathematical Modeling. Furthermore, we wish to acknowledge the support of the US Army Research Office under grant W911NF-05-1-0301 to Arizona State University.

REFERENCES

[1] J. Allen and A. Berkeley. Image method for efficiently simulating small-room acoustics. *J. Acoust. So. Amer.*, 65(4):943–950, Apr. 1979.

[2] A. Antoulas and D. Sorensen. Approximation of large-scale dynamical systems: An overview. Technical report, Rice University, 2001.

[3] A. Berkhout, D. de Vries, and P. Vogel. Acoustic control by wave field synthesis. *J. Acoust. Soc. Am.*, 93(5):2764–2778, 1993.

[4] M. Bertram, E. Deines, J. Mohring, J. Jegorovs, and H. Hagen. Phonon tracing for auralization and visualization of sound. In *IEEE Visualization*, Minneapolis, MN, October 2005.

[5] J. Borish. Extension of the image model to arbitrary polyhedra. *J. Acoust. So. Amer.*, 75(6):1827–1836, 1984.

[6] L. Cremer and H. Müller. *Die wissenschaftlichen Grundlagen der Raumakustik, Band I*. S. Hirzel Verlag Stuttgart, 1978. 2. völlig neubearbeitete Auflage.

[7] E. Deines, F. Michel, M. Bertram, H. Hagen, and G. Nielson. Visualizing the phonon map. In *Eurographics / IEEE-VGTC Symposium on Visualization*, Lisbon, Portugal, Mai 8-10 2006.

[8] T. A. Funkhouser, I. Carlbom, G. Elko, G. P. M. Sondhi, and J. West. A beam tracing approach to acoustic modeling for interactive virtual environments. In *Computer Graphics (SIGGRAPH 98)*, pages 21–32, Orlando, FL, July 1998.

[9] T. A. Funkhouser, P. Min, and I. Carlbom. Real-time acoustic modeling for distributed virtual environments. In *Computer Graphics (SIGGRAPH 99)*, pages 365–374, Los Angeles, August 1999.

[10] W. Hackbusch. *Integralgleichungen, Theorie und Numerik*. Teubner Verlag, 1989.

[11] H. W. Jensen. Global illumination using photon maps. In *Rendering Techniques '96 (Proceedings of the 7th Eurographics Workshop on Rendering)*, pages 21–30, 1996.

[12] H. W. Jensen and P. H. Christensen. Efficient simulation of light transport in scene with participating media using photon maps. In *Computer Graphics (SIGGRAPH 98)*, pages 311–320, July 1998.

[13] B. Kapralos, M. Jenkin, and E. Millios. Sonel mapping: Acoustic modeling utilizing an acoustic version of photon mapping. In *IEEE International Workshop on Haptics Audio Visual Environments and their Applications (HAVE 2004)*, Ottawa, Canada, October 2-3 2004.

[14] B. Klehs and T. Sporer. Wave field synthesis in the real world part 1: In the living room. In *114th AES Convention*, Amsterdam, March 22 - 25 2003.

[15] H. Knobloch and H. Kwakernaak. *Lineare Kontrolltheorie*. Springer-Verlag, 1985.

[16] U. Krockstadt. Calculating the acoustical room response by the use of a ray tracing technique. *Journal of Sound and Vibrations*, 8(18):118–125, 1968.

[17] U. Kulowski. Algorithmic representation of the ray tracing technique. *Applied Acoustics*, 18:449–469, 1984.

[18] M. Monks, B. Oh, and J. Dorsey. Acoustic simulation and visualization using a new unified beam tracing and image source approach. In *Convention of the Audio Engineering Society*. ACM, 1996.

[19] I. O. of Standardization (ISO). Acoustics – measurement of the reverberation time of rooms with reference to other acoustical parameters. 1997.

[20] K. Olsson. Model order reduction in FEMLAB by dual rational Arnoldi, 2002.

[21] M. Vorländer. Simulation of the transient and steady-state sound propagation in rooms using a new combined ray-tracing/image-source algorithm. *J. Acoust. So. Amer.*, 86(1):172–178, 1989.

[22] K. Zhou and J. Doyle. *Essentials of robust control*. Prentice-Hall inc., 1998.

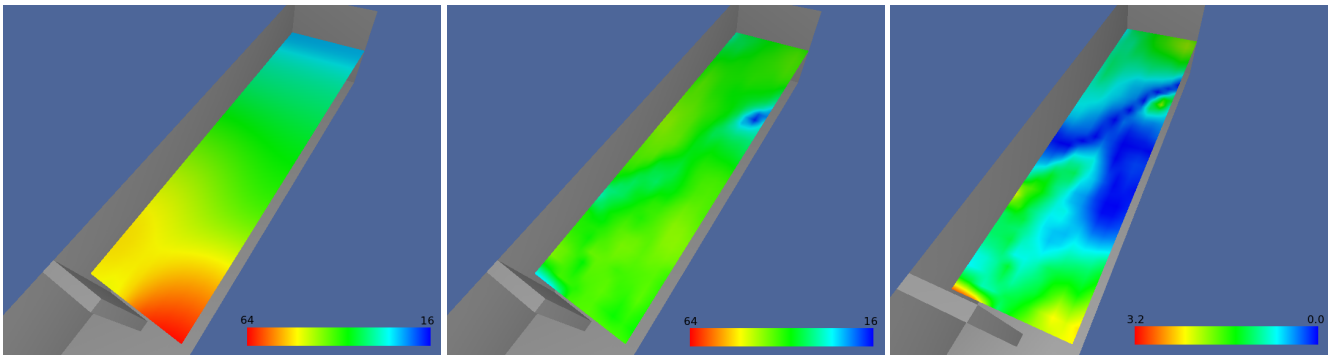

(a) (b) (c)

Fig. 9. Gain visualization (values in dB). (a) FEM simulation, (b) phonon tracing, and (c) the relative error by wave number k=3.

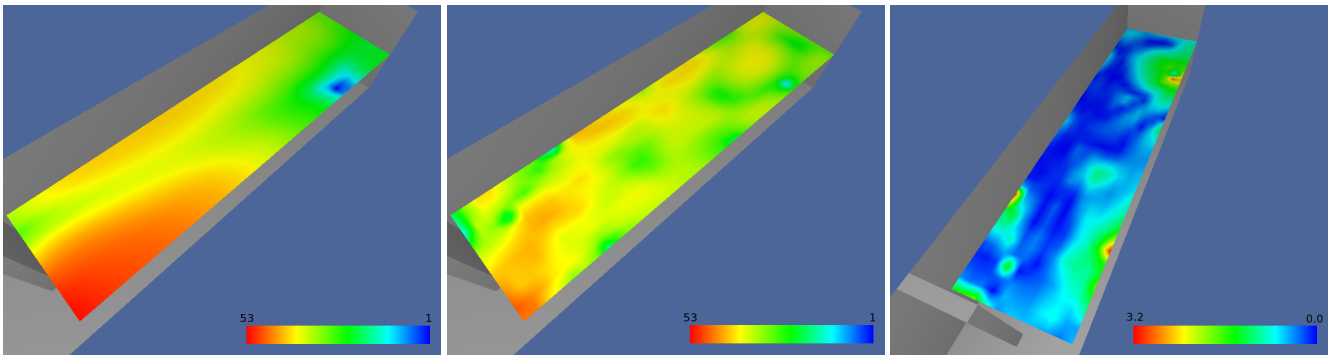

(a) (b) (c)

Fig. 10. Gain visualization (values in dB). (a) FEM simulation, (b) phonon tracing, and (c) the relative error by wave number k=6.

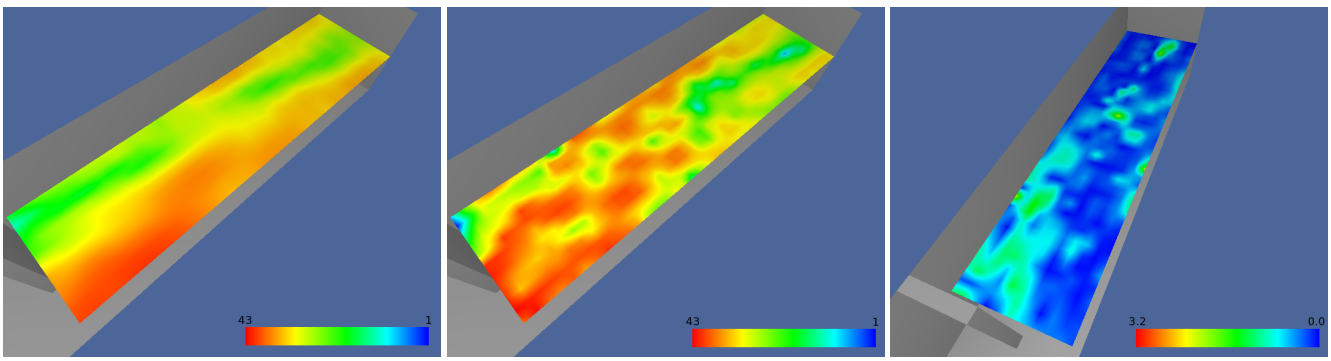

(a) (b) (c)

Fig. 11. Gain visualization (values in dB). (a) FEM simulation, (b) phonon tracing, and (c) the relative error by wave number k=12.